An RNA-binding switch drives ribosome biogenesis and tumorigenesis downstream of RAS oncogene

Muhammad S. Azman[1], Martin Dodel[1], Federica Capraro[1,2], Rupert Faraway[3,4], Maria Dermit[1], Wanling Fan[1], Jernej Ule[3,4], & Faraz K. Mardakheh[1*].

1: *Centre for Cancer Cell and Molecular Biology, Barts Cancer Institute, Queen Mary University of London, Charterhouse square, London EC1M 6BQ, United Kingdom.*
2: *Randall Centre for Cell and Molecular Biophysics, King's College London, London, SE1 1UL, United Kingdom.*
3: *The Francis Crick Institute, 1 Midland Road, London NW1 1AT, United Kingdom.*
4: *Department of Neuromuscular Diseases, UCL Queen Square Institute of Neurology, Queen Square, London WC1N 3BG, United Kingdom.*
***:** *Correspondence: f.mardakheh@qmul.ac.uk*

Summary

Oncogenic RAS signaling reprograms gene expression through both transcriptional and post-transcriptional mechanisms. While transcriptional regulation downstream of RAS is relatively well-characterized, how RAS post-transcriptionally modulates gene expression to promote malignancy is unclear. Using quantitative RNA Interactome Capture analysis, we reveal that oncogenic RAS signaling reshapes the RNA-bound proteomic landscape of cancer cells, with a network of nuclear proteins centered around Nucleolin displaying enhanced RNA-binding activity. We show that Nucleolin is phosphorylated downstream of RAS, which increases its binding to pre-ribosomal-RNA (rRNA), boosts rRNA production, and promotes ribosome biogenesis. This Nucleolin-dependent enhancement of ribosome biogenesis is crucial for RAS-induced cancer cell proliferation, and can be targeted therapeutically to inhibit tumor growth. Our results reveal that oncogenic RAS signaling drives ribosome biogenesis by regulating the RNA-binding activity of Nucleolin, and highlights the crucial role of this process in RAS-mediated tumorigenesis.

Introduction

RAS genes are amongst the most mutated proto-oncogenes in human cancers, with around 20% of all malignancies estimated to harbor oncogenic mutation in one of the three highly homologous *KRAS*, *NRAS*, or *HRAS* genes (Prior et al., 2020). The encoded RAS proteins are small GTPases which function as molecular switches that regulate several downstream kinase signaling pathways, including the ERK1/2 (also known as the RAS-MAPK cascade), and the PI3K-AKT pathways (Malumbres and Barbacid, 2003). Oncogenic mutations in RAS result in constitutive activation of these downstream kinase signaling pathways, which phosphorylate a plethora of cellular substrates, including a number of transcription factors, ultimately resulting in significant changes in the gene expression profile that promote various aspects of malignancy (Pylayeva-Gupta et al., 2011). Although this transcriptional regulation has been shown to play a key role in RAS induced tumorigenesis, recent studies have revealed that a significant degree of gene expression dysregulation that occurs in cancers is post-transcriptional (Nusinow et al., 2020). However, how oncogenic RAS signaling modulates gene expression post-transcriptionally remains largely unclear.

RNA-binding Proteins (RBPs) are the main post-transcriptional regulators of gene expression, controlling all aspects of the RNA life-cycle from synthesis to degradation (Gerstberger et al., 2014). Numerous studies have revealed a key role for many RBPs in cancer development and progression (Kang et al., 2020). These RBPs coordinate diverse aspects of post-transcriptional regulation, including splicing (Fish et al., 2021), post-transcriptional modifications (Barbieri et al., 2017), transport (Dermit et al., 2020), translation (Truitt et al., 2015), and turnover of various types of RNA (Yu et al., 2020). The recent advent of RNA Interactome Capture (RIC) methods, which allow global unbiased identification of proteins that are directly bound by RNA *in vivo*, has transformed our understanding of RBPs (Baltz et al., 2012; Castello et al., 2012; Queiroz et al., 2019; Trendel et al., 2019). Cumulatively, RIC studies have significantly expanded the catalogue of known RBPs, with around 10% of the human proteome having been demonstrated to bind RNA. These include not only 'conventional' RBPs, which contain at least one classical globular RNA-binding Domain (RBD), but also 'non-conventional' RBPs which lack any apparent RBDs (Hentze et al., 2018). When combined with quantitative proteomics, RIC can also be used for quantifying changes in the RNA-bound proteome (RBPome), thus allowing systematic study of RNA-binding dynamics (Garcia-Moreno et al., 2019; Sysoev et al., 2016). However, a comprehensive understanding of how oncogenic signaling pathways dynamically modulate the RBPome is still lacking.

Here, we devised a quantitative whole-transcriptome RIC approach, in order to define the impact of oncogenic RAS signaling on the RBPome of mouse Pancreatic Ductal Adenocarcinoma (PDAC) cells. We focused on PDAC, as nearly all its cases harbor oncogenic *KRAS* mutations, highlighting a key role for RAS in the etiology of the disease (Waters and Der, 2018). Our results reveal that through activation of downstream Erk1/2 signaling, oncogenic Kras extensively remodels the RBPome of PDAC cells, with various conventional RBPs

exhibiting enhanced RNA association, whilst non-conventional RBPs dissociate from RNA. Although the many of the observed alterations in the RBPome are due to changes in the expression of RBPs, some RBPs show modulations in their RNA-binding activity. Specifically, a network of conventional RBPs that includes the nucleolar protein Nucleolin (Ncl), exhibits a significant enhancement in their RNA-binding activity upon oncogenic Kras induction. Using quantitative phospho-proteomics, we reveal that several of these RBPs, including Ncl, are phosphorylated downstream of Erk1/2. Phosphorylation of Ncl acts to enhance its binding to pre-ribosomal-RNA (pre-rRNA), which in turn boosts rRNA synthesis and promotes ribosome biogenesis downstream of oncogenic Kras. Crucially, we demonstrate that the enhancement of ribosome biogenesis by Ncl is essential for oncogenic Kras-induced PDAC cell proliferation and tumorigenesis, and can be targeted therapeutically to inhibit PDAC growth, *in vivo*. Our findings reveal a switch in the RNA-binding activity of Ncl, triggered by phosphorylation downstream of Erk1/2, which governs rRNA synthesis and ribosome biogenesis, and demonstrate a key targetable role for this process in RAS-mediated tumors.

Results

Oncogenic Kras reshapes the RNA-binding landscape of mouse PDAC cells

To study oncogenic Kras signaling, we employed tumor cells from an inducible mouse model of PDAC (iKras), in which oncogenic $Kras^{G12D}$ expression can be controlled by administration of doxycycline (Ying et al., 2012). We confirmed that removal of doxycycline and the consequent loss of $Kras^{G12D}$ expression resulted in downregulation of Erk1/2 signaling in this model (Figure S1A & S1B). Conversely, addition of doxycycline to doxycycline-withdrawn cells induced $Kras^{G12D}$ expression and triggered Erk1/2 activation (Figure S1C and S1D). To study the RBPome, we employed Orthogonal Organic Phase Separation (OOPS), a whole-transcriptome RIC method which uses UV-C crosslinking coupled with phenol-chloroform based phase separation to purify *in vivo* crosslinked RNA-Protein moieties (Queiroz et al., 2019). We validated that OOPS specifically enriched for crosslinked RBPs (Figure S1E & S1F). We then devised a quantitative RIC (qRIC) approach by combining OOPS with Stable Isotope Labelling by Amino acids in Culture (SILAC) (Ong and Mann, 2006), allowing us to measure changes in the RBPome upon induction of $Kras^{G12D}$ expression (Figure 1A). Inducing $Kras^{G12D}$ expression resulted in a significant increase in the RNA-bound levels of 73 proteins, whilst 101 proteins showed a significant decrease (Figure 1B & Dataset S1). Category enrichment analysis revealed that the majority of increased RNA-bound proteins were conventional RBPs, belonging to various RBP families involved in nuclear RNA processing and ribosome biogenesis (Figure 1C & Dataset S2). In contrast, the majority of decreased RNA-bound proteins were non-conventional RBPs such as metabolic enzymes and cytoskeletal proteins (Figure 1D & Dataset S3). Importantly, the effect of $Kras^{G12D}$ on the RBPome was largely abrogated upon treating the cells with Trametinib, a specific MEK kinase inhibitor which blocks Erk1/2 activation downstream of $Kras^{G12D}$ (Wright and McCormack, 2013), suggesting that the observed changes are largely dependent on Erk1/2 signaling (Figure 1E, S1G-H & Dataset S4).

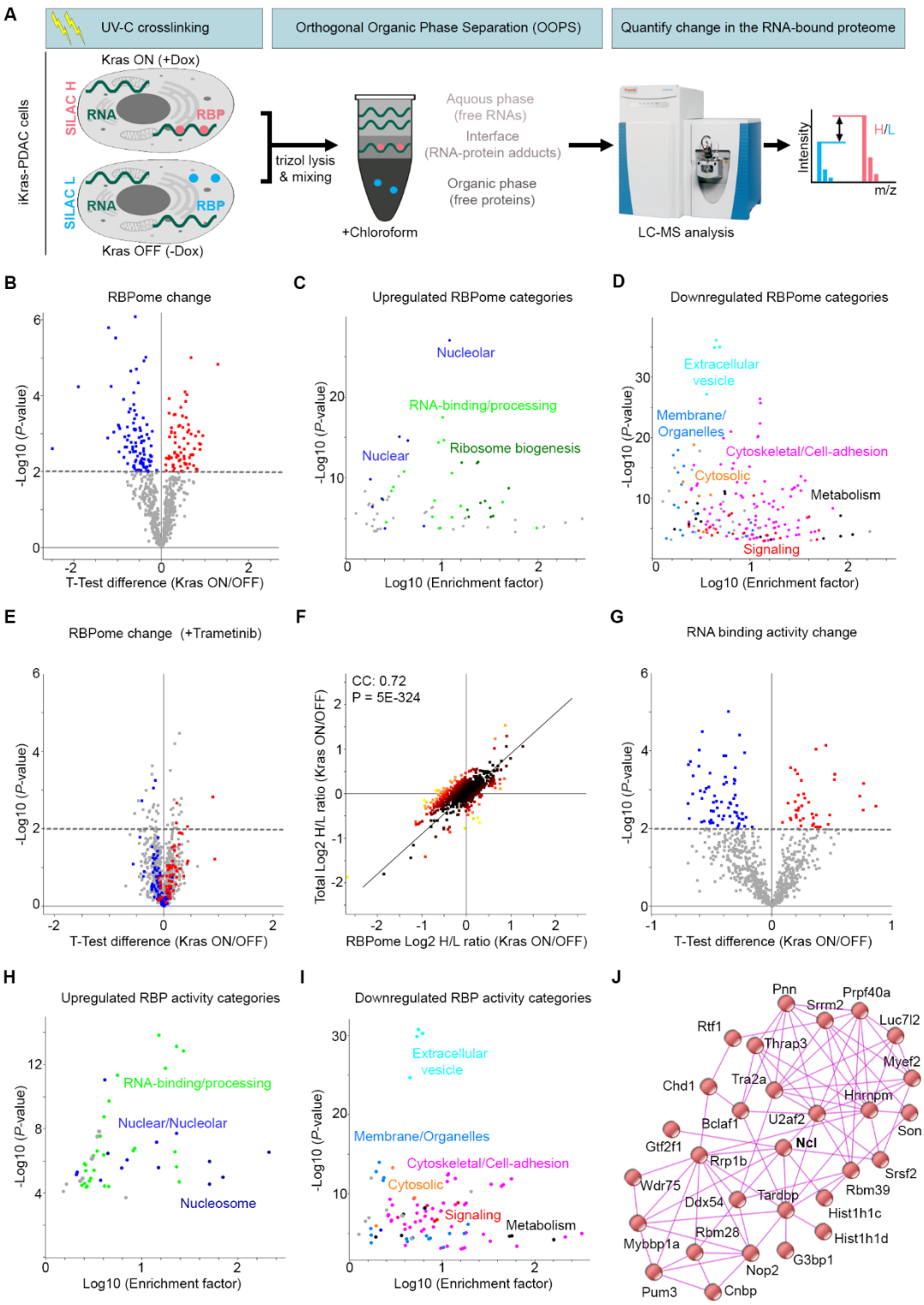

Figure 1: Kras^{G12D} reshapes the RBPome landscape of PDAC cells. (A) Experimental workflow for qRIC analysis of the RBPome in iKras PDAC cells. Heavy (H) and Light (L) SILAC labelled iKras cells, with or without Kras^{G12D}, were subjected to UV-C crosslinking, TRIzol lysis, mixing of differentially labelled conditions, and OOPS analysis as in (Queiroz et al., 2019) . RNA-crosslinked proteins, which separate into the interface, were then extracted and subjected to Trypsin digestion and liquid chromatography coupled with mass spectrometry analysis. The SILAC (H/L) ratio values revealed Kras^{G12D}-regulated changes in the RBPome. **(B)** Volcano plot of changes in the RBPome following Kras^{G12D} induction. RBPome changes were quantified, as described in (A), from 6 independent qRIC experiments (Dataset S1), using a one-sample t-test analysis. 73 proteins were upregulated in the RNA-bound fraction (red), whilst 101 RBPs showed a significant decrease (blue) ($P < 0.01$). **(C)** Fisher's exact test analysis of protein categories that are over-represented amongst the upregulated RBPome (FDR < 0.02). Each

data point represents a category from Gene Ontology (GO) and Kyoto Encyclopedia of Genes & Genome (KEGG) databases, with functionally similar categories highlighted with the same colors (Dataset S2). **(D)** Fisher's exact test analysis of protein categories that are over-represented amongst the downregulated RBPome (FDR < 0.02). Each data point represents a category from GO and KEGG databases, with functionally similar categories highlighted with the same colors (Dataset S3). **(E)** Volcano plot of $Kras^{G12D}$-driven changes in the RBPome in presence of Trametinib (10 nM). RBPome changes in presence of Trametinib were quantified from 4 independent qRIC experiments, using a one-sample t-test analysis (P < 0.01), with significantly increased (red) or decreased (blue) proteins from (B) highlighted on the plot (Dataset S4). **(F)** SILAC Total proteome changes following $Kras^{G12D}$ induction were measured and plotted against RBPome changes from (B). Pearson's Correlation Coefficient (CC) and significance of correlation (P) between the total proteome and the RBPome changes were calculated and displayed on the graph. **(G)** Volcano plot of changes in the RNA-binding activity following $Kras^{G12D}$ induction. RBPome ratio changes from (B) were normalized to total proteome ratio changes from (F) to calculate changes in the RNA-binding activity (Dataset S5), using a one-sample t-test analysis. 40 proteins showed an increase in their RNA-binding activity (red), whilst 65 proteins exhibited a decrease (blue) (P < 0.01). **(H)** Fisher's exact test analysis of categories that are over-represented amongst the proteins with enhanced RNA-binding activity (FDR < 0.02). Each data point represents a category from GO and KEGG databases, with functionally similar categories highlighted with the same colors (Dataset S6). **(I)** Fisher's exact test analysis of categories that are over-represented amongst the proteins with diminished RNA-binding activity (FDR < 0.02). Each data point represents a category from GO and KEGG databases, with functionally similar categories highlighted with the same colors (Dataset S7). **(J)** Interactome network analysis of proteins with enhanced RNA-binding activity from (G), using the STRING physical interactions database (Franceschini et al., 2013).

Next, we investigated the mechanisms of RBPome modulation in response to induction of $Kras^{G12D}$ expression. Dysregulation of RBPs in cancer is primarily thought to be brought about by changes in their expression (Pereira et al., 2017). However, signaling pathways have also been shown to modulate the activity of some RBPs through post-translational modifications (Hong et al., 2017; Matter et al., 2002; Tripathi et al., 2010). To assess these two possibilities, we performed SILAC based total proteomics on the iKras PDAC cells, with or without the induction of $Kras^{G12D}$ expression. We observed a strong overall correlation between changes in the RBPome and the total proteome, suggesting that the majority of variation in the RBPome is likely reflective of changes in the expression levels of RBPs (Figure 1F). However, not all changes were correlative, so to specifically reveal alterations in the RBPome that were independent of protein expression modulations, we normalized the RBPome SILAC ratio values to those of the total proteome. Analysis of this RBPome to total normalized ratio value thus revealed changes in the RNA-binding activities of RBPs in response to $Kras^{G12D}$ induction. We observed a significant increase in the RNA-binding activity of 40 proteins, coupled with a significant decrease in the RNA-binding activity of 65 proteins (Figure 1G & Dataset S5). Similar to the RBPome analysis, category enrichment revealed that the majority of proteins with increased RNA-binding activity were conventional RBPs belonging to various nuclear protein families (Figure 1H & Dataset S6), whilst the majority of proteins with decreased RNA-binding activity were non-conventional cytoplasmic RBPs belonging mostly to metabolic and cytoskeletal protein families (Figure 1I & Dataset S7). Interactome analysis of the RBPs with increased RNA-binding activity revealed that many of them are known to physically associate with one another (Figure 1J). Several of these RBPs such as Ncl, Rrp1b, Wdr75, Nop2, and Mybbp1a are known regulators of ribosome biogenesis (Chamousset et al., 2010; de Beus et

al., 1994; Liu et al., 2017; Moudry et al., 2021; Ugrinova et al., 2018). Together, these results
185 reveal that Kras^{G12D} mediated Erk1/2 activation reshapes the RBPome landscape of PDAC cells, with a network of nuclear RBPs, which includes Ncl and several other ribosome biogenesis factors, exhibiting a significant enhancement in their RNA-binding activity.

Oncogenic Kras signaling enhances the RNA-binding activity of Ncl through phosphorylation

190 We next set out to investigate the mechanism by which Erk1/2 signaling modulated the RNA-binding activity of RBPs downstream of Kras^{G12D}. Erk1/2 is a major cellular kinase that can directly or indirectly phosphorylate a plethora of downstream cellular substrates (Yoon and Seger, 2006). We therefore hypothesized that some of the changes in RNA-binding activity could be mediated via Erk1/2 dependent phosphorylation of RBPs. To reveal Erk1/2-
195 dependent phosphorylation changes that are brought about by Kras^{G12D} induction, we carried out a multi-variate quantitative phospho-proteomics analysis of iKras PDAC cells, using Tandem Mass Tagging (TMT) (McAlister et al., 2012) (Dataset S8). Of a total of 7,478 phosphorylations identified, 872 were found to be significantly increased upon Kras^{G12D} induction (Figure 2A). As expected, phospho-motif analysis revealed the ERK substrate motif
200 to be highly over-represented amongst these phosphorylation sites, but motifs for a number of other kinases such as Casein Kinase I (CK1) and Casein Kinase II (CK2) were also significantly over-represented, albeit to a lesser extent (Figure S2A). Several RBPs whose RNA-binding activity was significantly enhanced upon Kras^{G12D} induction were amongst the phosphorylation targets of Kras^{G12D}, often found to be phosphorylated on multiple residues
205 (Figure 2A & 2B). The impact of Kras^{G12D} induction on the phospho-proteome was completely abrogated by treating the cells with Trametinib (Figure 2C), suggesting that Erk1/2 signaling is the principal driver of phosphorylation events downstream of Kras^{G12D} in iKras PDAC cells. These findings are in agreement with previous studies which showed cell-autonomous Kras^{G12D} signaling in PDAC to be primarily mediated via Erk1/2 (Tape et al., 2016), and reveal
210 that a number of RBPs, whose RNA-binding activity is enhanced downstream of Kras^{G12D}, also undergo phosphorylation downstream of Erk1/2.

Amongst the Kras^{G12D} regulated RBPs which were significantly phosphorylated downstream of Erk1/2, Ncl was strongly phosphorylated on 4 closely situated Serine residues (S28, S34,
215 S40, and S41) within its N-terminal region (Figure 2B). This region, consisted of acidic-rich regions interspersed with stretches of basic residues, is predicted to be largely disordered (Jumper et al., 2021). It is also well-known to undergo phosphorylation by multiple kinases (Tajrishi et al., 2011), but no direct link between Ncl phosphorylation and Erk1/2 signaling has been reported. Phospho-motif analysis revealed that the identified phosphorylation sites are
220 not direct Erk1/2 targets, but most likely phosphorylated by CK2 (Figure 2D), which is well-known to physically associate with and phosphorylate Ncl (Caizergues-Ferrer et al., 1987; Li et al., 1996). Importantly, CK2 has been shown to be activated downstream of ERK1/2 signaling (Ji et al., 2009), which is in agreement with our phospho-motif analysis of the Kras^{G12D} enhanced phosphorylation sites (Figure S2A). Accordingly, we could demonstrate by
225 using a specific phospho-CK2-Substrate antibody mix that Kras^{G12D} induction enhanced CK2 activity in an Erk1/2-dependent manner in iKras PDAC cells (Figure S2B-E). These findings

suggest that Erk1/2 activation downstream of Kras^{G12D} increases CK2 activity, leading to enhanced phosphorylation of Ncl on S28, S34, S40, and S41.

To reveal whether the observed phosphorylations and the enhancement of the RNA-binding activity of Ncl were causally linked, we generated phospho-defective and phospho-mimicking mutants of Ncl, in which the four identified residues were mutated either to Alanine (S4A), or Aspartic acid (S4D), respectively. Myc-tagged versions of these mutants along with the wild-type (WT) control were ectopically expressed in iKras PDAC cells, and the cells were subjected to OOPS analysis. The interface, which contains RNA-bound proteins, along with the organic phase, which contains free proteins, were then analyzed by western blotting with an anti-Myc antibody. While no variations were observed between the levels of Ncl in the organic phase, the levels of the phospho-mimicking (S4D) mutant exhibited a significant increase in the interface, suggesting that its RNA-binding activity must be significantly increased (Figure 2E & 2F). These results suggest that phosphorylation of Ncl on S28, S34, S40, and S41 acts to enhance its RNA-binding activity downstream of Kras^{G12D}.

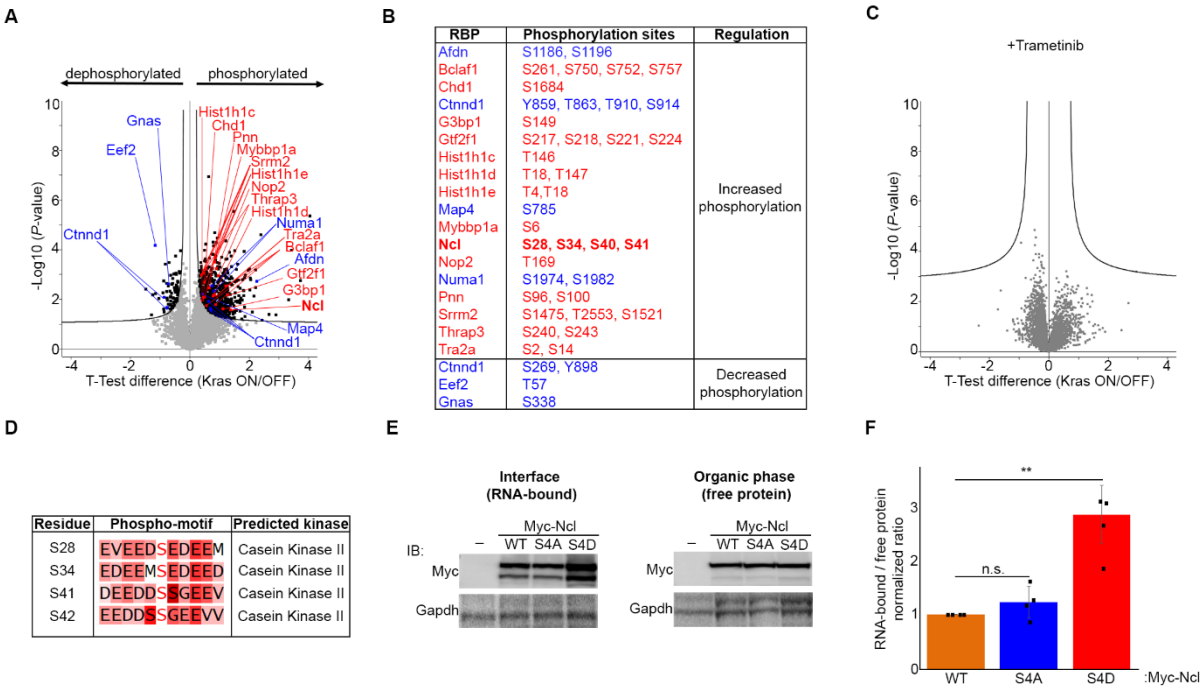

RBP	Phosphorylation sites	Regulation
Afdn	S1186, S1196	Increased phosphorylation
Bclaf1	S261, S750, S752, S757	
Chd1	S1684	
Ctnnd1	Y859, T863, T910, S914	
G3bp1	S149	
Gtf2f1	S217, S218, S221, S224	
Hist1h1c	T146	
Hist1h1d	T18, T147	
Hist1h1e	T4,T18	
Map4	S785	
Mybbp1a	S6	
Ncl	**S28, S34, S40, S41**	
Nop2	T169	
Numa1	S1974, S1982	
Pnn	S96, S100	
Srrm2	S1475, T2553, S1521	
Thrap3	S240, S243	
Tra2a	S2, S14	
Ctnnd1	S269, Y898	Decreased phosphorylation
Eef2	T57	
Gnas	S338	

Residue	Phospho-motif	Predicted kinase
S28	EVEEDSEDEEM	Casein Kinase II
S34	EDEEMSEDEED	Casein Kinase II
S41	DEEDDSSGEEV	Casein Kinase II
S42	EEDDSSGEEVV	Casein Kinase II

Figure 2: The RNA-binding activity of Ncl is enhanced upon its phosphorylation downstream of Kras^{G12D}-induced Erk1/2 signaling. (A) Volcano plot of phosphorylation changes in iKras PDAC cells in response to Kras^{G12D} induction. Phospho- to total proteomic changes were quantified from 3 independent replicates of doxycycline treated vs. untreated cells, via TMT (Dataset S8). 872 phosphorylations were found to be significantly increased, while 82 phosphorylations were significantly decreased (FDR < 0.05). Significantly changing phosphorylations on RBPs whose RNA-binding activity was significantly increased (red) or decreased (blue) as per Figure 1G are highlighted on the plot. **(B)** List of significantly increased or decreased phosphorylation sites on the RBPs whose RNA-binding activity was enhanced (red) or reduced (blue) upon Kras^{G12D} induction. **(C)** Volcano plot of phosphorylation changes in iKras PDAC cells in response to Kras^{G12D} induction in presence of Trametinib (10 nM). Phospho- to total proteomic changes were quantified from 3 independent replicates of doxycycline + Trametinib treated vs. untreated cells (Dataset S8). No phosphorylations were found to be significantly changing upon Kras^{G12D} induction in presence of Trametinib (FDR < 0.05). **(D)** Phospho-motif kinase prediction analysis of Kras^{G12D}-induced Ncl phosphorylation sites, using NetworKIN (Linding et al., 2008). **(E)** OOPS analysis of the RNA-binding activity of WT, Phospho-defective (S4A), and phospho-mimicking (S4D) mutants of Ncl. Vectors encoding

Myc-tagged WT, S4A, and S4D Ncl were transiently expressed in iKras PDAC cells, before OOPS and western blot analysis of the interface (RNA-bound) and the organic phase (free protein) fractions with anti-Myc antibody. Gapdh, which also binds RNA (Dataset S1), was blotted as loading control. **(E)** Quantification of normalized RNA-bound to free Myc-Ncl ratio values from (E), as measures of RNA-binding activity (n = 4) (**: P < 0.01; n.s.: not significant).

Transcriptome-wide iCLIP studies reveal Ncl to be primarily associated with pre-rRNA

After revealing that the RNA-binding activity of Ncl is enhanced by phosphorylation downstream of Kras^{G12D}, we set out to determine the full spectrum of RNAs which are bound by Ncl and their dynamics in response to Kras^{G12D}-dependent phosphorylation. Although predominantly known to be localized to the nucleolus, where it regulates several steps of ribosome biogenesis, Ncl has also been shown to have diverse extra-nucleolar functions in the nucleoplasm, cytoplasm, as well as the cell-surface (Ugrinova et al., 2018). These include regulation of chromatin architecture (Angelov et al., 2006; Erard et al., 1988), microRNA processing (Pichiorri et al., 2013; Pickering et al., 2011), translation (Abdelmohsen et al., 2011; Takagi et al., 2005), as well as mRNA turnover (Sengupta et al., 2004; Zhang et al., 2006). In addition, cell-surface localized Ncl has been shown to be involved in regulation of cell adhesion and transmembrane signaling (Losfeld et al., 2009; Reyes-Reyes and Akiyama, 2008). In order to identify the full repertoire of RNAs which directly interact with Ncl, and reveal the impact of Kras^{G12D}-dependent phosphorylation on their association with Ncl, we performed individual-nucleotide resolution UV crosslinking and immunoprecipitation (iCLIP) (Konig et al., 2010). Ncl-RNA complexes were purified by immunoprecipitation with an anti-Myc-tag antibody, from iKras PDAC cells that ectopically expressed Myc-tagged WT, S4A, or S4D mutants of Ncl, or a mock transfected negative control. Western blot analysis revealed that the ectopic proteins were expressed at around 50% of the endogenous levels, ruling out potential artefacts due to high levels of overexpression (Figure S3A & S3B). Moreover, little mapped iCLIP reads were identified from the negative control iCLIP samples, as opposed to the Myc-Ncl samples, suggesting that the identification of interacting RNAs was highly specific (Figure S3C). More than 70% of all the Myc-Ncl iCLIP mapped reads corresponded to the ribosomal-DNA (rDNA) locus, which codes for a long primary transcript known as the 47S pre-rRNA that is ultimately processed into 18S, 5.8S, and 28S rRNAs (Figure 3A). No significant difference between WT and the phospho-mutants was observed, suggesting that phospho-regulation of Ncl by Kras^{G12D} does not affect its repertoire of RNA substrates (Figure 3A). In agreement with these results, immunofluorescence analysis revealed that ectopically expressed Myc-tagged WT, S4A, and S4D mutants of Ncl were exclusively localized to the nucleolus (Figure 3B). Localization of ectopic Myc-Ncl was in complete accordance with endogenous Ncl, which was also found to be exclusively nucleolar, irrespective of Kras^{G12D} status (Figure S3D). Together, these results suggest that Ncl is primarily localized to the nucleolus of iKras PDAC cells, irrespective of its Kras^{G12D}-dependent phosphorylation status, and predominantly binds pre-rRNA.

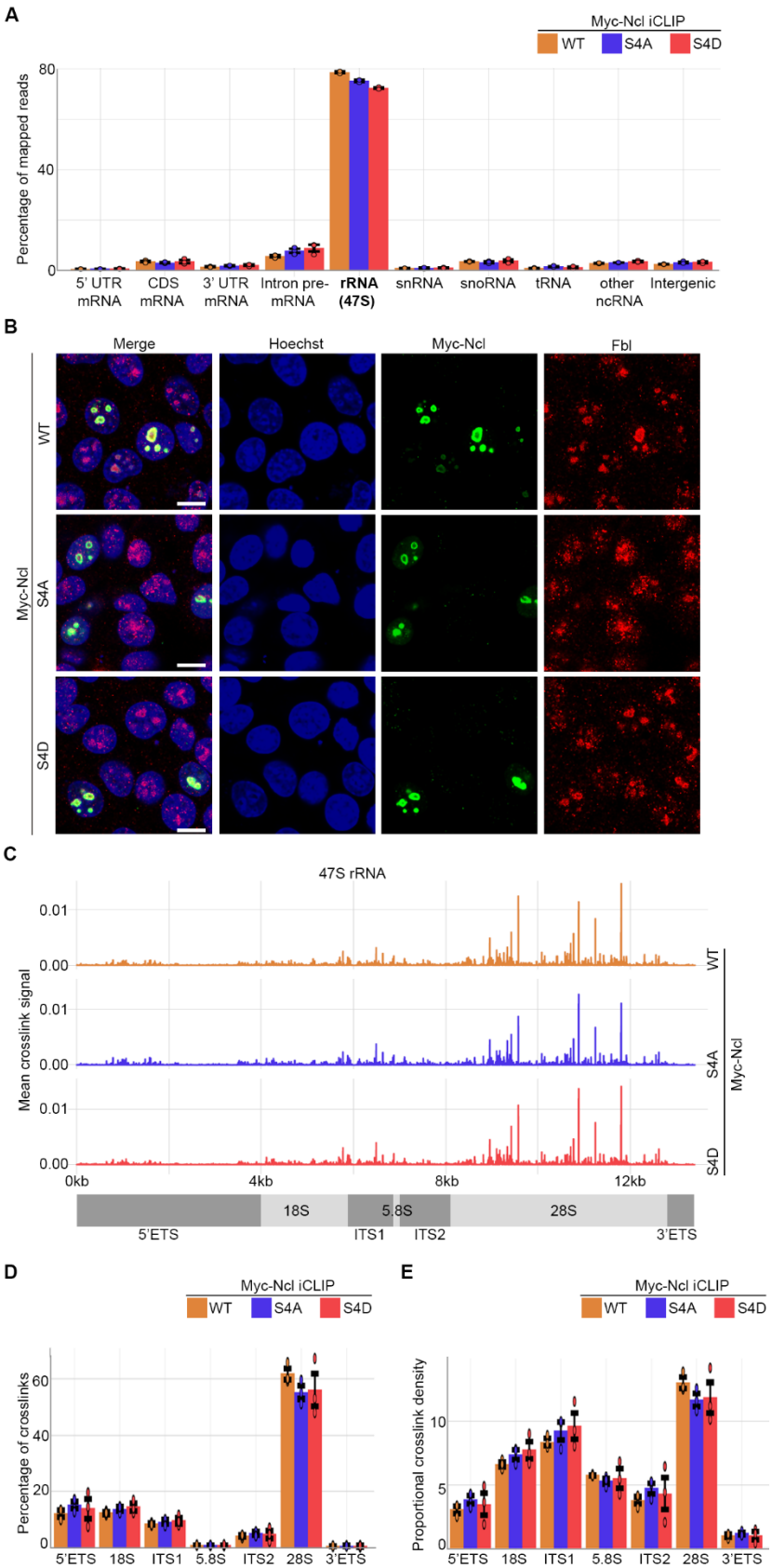

Figure 3: Ncl is predominantly bound to pre-rRNA, irrespective of its phosphorylation status. (A) Percentage of mapped reads belonging to different types of RNA from three independent iCLIP replicate experiments of WT, S4A, and S4D Myc-Ncl. **(B)** Immunofluorescence analysis of WT, S4A, and S4D Myc-Ncl subcellular localization. IKras PDAC cells ectopically expressing either WT, S4A, or S4D Myc-Ncl were fixed and immunostained with anti-Myc-tag antibody, along with anti-Fibrillarin (Fbl) antibody as a Nucleolar marker, and Hoechst, followed by confocal microscopy analysis. Scale bar = 10 µm. **(C)** Distribution of WT, S4A, and S4D Myc-Ncl crosslink sites across the annotated 47S pre-rRNA genomic region. Peak heights represent mean crosslink intensities from three independent iCLIP replicate experiments. **(D)** Quantification of the percentage of crosslinks in each region of the 47S pre-rRNA for WT, S4A, and S4D Myc-Ncl. Percentage of crosslinks relative to 47S total were quantified from three independent iCLIP experiments. **(E)** Quantification of the proportional density of crosslinks in each region of the 47S pre-rRNA for WT, S4A, and S4D Myc-Ncl. Proportional density was calculated from three independent iCLIP experiments by normalizing the number of crosslinks in each region to the sequence length of that region.

Although Kras^{G12D}-dependent phosphorylation of Ncl does not affect its primary association with pre-rRNA, the enhancement of the RNA-binding activity could be resulting in generation of novel Ncl binding sites on the pre-rRNA. Alternatively, Ncl could be binding to exactly the same sites, but with higher affinity. To differentiate between these possibilities, we analyzed

350 the distribution of Ncl crosslink sites within the pre-rRNA. 47S pre-rRNA contains the sequences of 18S, 5.8S, and 28S rRNAs, flanked by two external transcribed spacers at each end (5'ETS and 3'ETS), as well as two Internal transcribed spacers (ITS1 and ITS2) that are situated between 18S, 5.8S, and 28S. During rRNA processing, these spacer sequences are removed in a step-by-step manner via the action of different endo- and exo-ribonucleases
355 (Turowski and Tollervey, 2015). WT Ncl showed binding throughout the length of 47S pre-rRNA, with several spikes of crosslinked sites detected in various regions (Figure 3C). No difference between the crosslinking patterns of the WT and the phospho-mutants were observed, suggesting that phosphorylations do not change the binding pattern of Ncl on pre-rRNA (Figure 3C). Accordingly, quantification of the percentage as well as the density of Ncl
360 crosslinks within each pre-rRNA region revealed no differences between WT Ncl and the phospho-mutants (Figure 3D & 3E). Collectively, these results suggest that the Kras^{G12D}-dependent phosphorylations of Ncl do not affect its pattern of binding to pre-rRNA. We therefore conclude that the Kras^{G12D}-dependent phospho-regulation of Ncl must be acting to enhance its RNA-binding affinity, without affecting its RNA-binding specificity.

365

Ncl phosphorylation enhances rRNA synthesis and ribosome biogenesis

The predominant interaction of Ncl with pre-rRNA suggests that it must be primarily functioning in regulating ribosome biogenesis in iKras PDAC cells, so we next investigated the functional impact of Ncl phospho-regulation on controlling ribosome biogenesis downstream
370 of Kras^{G12D}. We first assessed the impact of Kras^{G12D} induction on nascent rRNA levels, using single-cell visualization of newly synthesized RNAs by 5-fluorouridine (FUrd) pulse-labeling (Percipalle and Louvet, 2012). Induction of Kras^{G12D} expression by addition of doxycycline to doxycycline-withdrawn cells triggered a strong accumulation of nascent RNA within the nucleolus of iKras PDAC cells. This accumulation was largely abrogated by short-term
375 treatment of the cells with a specific RNA polymerase I inhibitor (CX-5461), suggesting that the nucleolar nascent RNA signal must be largely comprised of newly synthesized rRNA (Figure S4A & S4B). Conversely, removal of doxycycline and the consequent loss of Kras^{G12D} expression resulted in a substantial reduction in nascent rRNA levels (Figure S4C & S4D), collectively demonstrating a strong dependence of rRNA synthesis on Kras^{G12D} expression.
380 Crucially, depletion of Ncl via two independent siRNA oligos abrogated nascent rRNA accumulation downstream of Kras^{G12D} (Figure 4A, 4B, & S4E). As an independent approach, we also measured the levels of unprocessed pre-rRNA by quantitative reverse transcription-PCR (RT-qPCR), using a probe against the 5'ETS region of 47S pre-rRNA which is removed at the first step of pre-rRNA processing (Pineiro et al., 2018). In agreement with the nascent RNA
385 imaging results, Kras^{G12D} expression resulted in an increase in the levels of unprocessed pre-rRNA, but this increase was abrogated upon Ncl depletion (Figure 4C). Together, these findings suggest that Kras^{G12D} acts to enhance pre-rRNA expression in a Ncl-dependent manner.

390 Synthesis of 47S pre-rRNA is a critical step in the regulation of eukaryotic ribosome biogenesis (Pelletier et al., 2018), so we next assessed whether the Ncl-dependent enhancement of pre-

rRNA levels by Kras^{G12D} leads to an increase in cellular ribosome levels. Time-course quantitative proteomics analysis of iKras PDAC cells using TMT revealed a significant accumulation of Ribosomal Proteins (RPs) in response to induction of Kras^{G12D} expression (Figure S4F & Dataset S9). Conversely, RPs were depleted over time in response to loss of Kras^{G12D} expression (Figure S4G & Dataset S10). Category enrichment analysis revealed that protein categories corresponding to RPs and rRNA processing were amongst the most depleted in response to Kras^{G12D} loss (Figure S4H & Dataset S11). Since RPs are known to be highly unstable unless incorporated into mature ribosomal subunits (Lam et al., 2007), their stable accumulation in response to Kras^{G12D} expression is indicative of higher ribosome levels. Crucially, Ncl depletion abrogated the stable accumulation of RPs in response to Kras^{G12D} expression, suggesting that enhancement of ribosome biogenesis downstream of Kras^{G12D} is dependent on Ncl (Figure 4D).

To determine whether the Erk1/2-dependent phosphorylation of Ncl plays a role in regulating pre-rRNA expression and ribosome biogenesis downstream of Kras^{G12D}, we evaluated the impact of phospho-defective (S4A) and phospho-mimicking (S4D) mutants of Ncl on nascent pre-rRNA levels, in presence or absence of Kras^{G12D}. In presence of Kras^{G12D}, iKras PDAC cells ectopically expressing either WT Ncl or the phospho-mutants exhibited accumulation of nascent rRNA in their nucleolus, though nascent rRNA levels were mildly but significantly decreased in S4A expressing cells (Figure 4E & 4F). Kras^{G12D} removal abrogated nascent rRNA levels in the WT and S4A mutant expressing cells, but the expression of the S4D mutant could rescue nascent rRNA expression in the absence of Kras^{G12D} (Figure 4E & 4F), suggesting that phosphorylation of Ncl is sufficient for enhancing nascent rRNA expression downstream of Kras^{G12D}. RT-qPCR analysis revealed that the S4D mutant caused a drastic accumulation of unprocessed pre-rRNA in the absence of Kras^{G12D} (Figure 4G). This accumulation far exceeded the pre-rRNA levels in presence of Kras^{G12D}, suggestive of a defect in pre-rRNA processing (Dermit et al., 2020). Based on these results, we conclude that the phospho-mimicking S4D mutant can enhance nascent pre-rRNA expression in the absence of Kras^{G12D}, but is defective in mediating the processing of pre-rRNA. Accordingly, quantitative proteomics analysis of iKras PDAC cells that ectopically expressed WT Ncl or the phospho-mutants revealed no S4D mediated rescue of ribosome biogenesis in the absence of Kras^{G12D} expression (Figure 4H). Together, these findings suggest that Ncl phosphorylation downstream of Kras^{G12D} acts to enhance pre-rRNA expression, but the subsequent processing of nascent pre-rRNA likely requires dephosphorylation of Ncl.

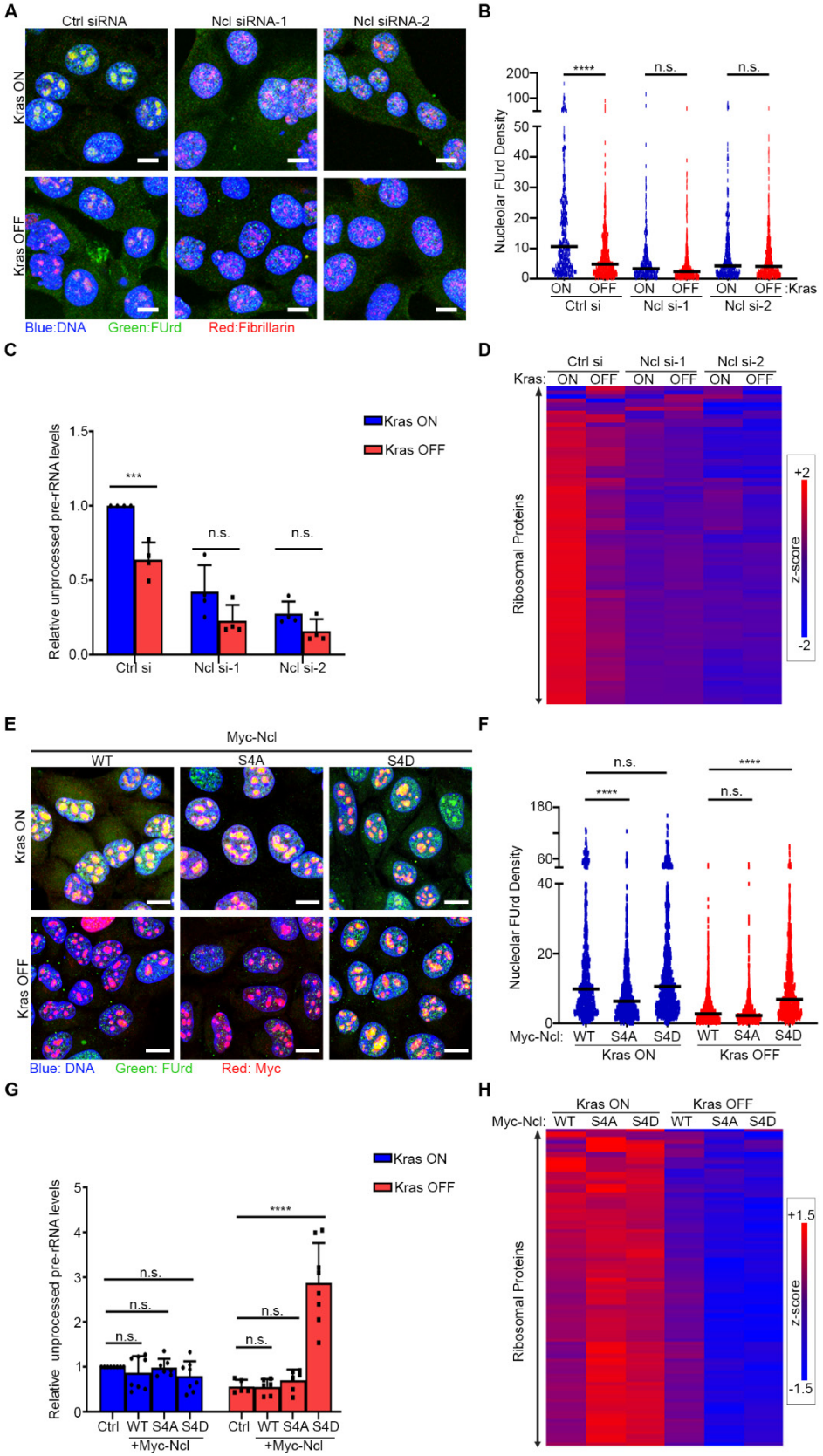

Figure 4: Kras^{G12D} promotes rRNA synthesis and ribosome biogenesis via Ncl. (A) Nascent RNA imaging in control and Ncl depleted iKras PDAC cells, in presence or absence of Kras^{G12D}. Cells were transfected with a non-
430 targeting control siRNA, or two independent siRNAs against Ncl, grown for 48hrs in presence or absence of doxycycline, before being subjected to pulse labeling with FUrd. Cells were then fixed and immunostained with anti-FUrd antibody (green) to visualize nascent RNA, along with anti-Fibrillarin (Fbl) antibody as a Nucleolar marker (red), and Hoechst (blue) as the Nuclear stain, followed by confocal microscopy analysis. Scale bar = 10

µm. **(B)** Quantification of Nucleolar FUrd levels in images from (A). FUrd fluorescence densities in single nucleoli were quantified from 182-220 individual cells per condition, combined from two independent biological replicate experiments (****: P < 0.0001; n.s.: not significant). **(C)** RT-qPCR analysis of 5'ETS-containing pre-rRNA transcript levels in control and Ncl depleted iKras PDAC cells, in presence or absence of $Kras^{G12D}$. Cells were transfected with a non-targeting control siRNA, or two independent siRNAs against Ncl, and grown for 48hrs in presence or absence of doxycycline, before RT-qPCR analysis with a specific probe against the mouse 5'ETS region. A probe against mouse Actb mRNA was used as loading control for normalization (n = 3) (***: P < 0.001; n.s.: not significant). **(D)** TMT quantitative analysis of RP levels in control and Ncl depleted iKras PDAC cells, in presence or absence of $Kras^{G12D}$. Cells were transfected with a non-targeting control siRNA, or two independent siRNAs against Ncl, and grown for 48hrs in presence or absence of doxycycline, before lysis and TMT-mediated quantitative proteomics analysis. Z-scores of TMT intensity changes for all identified RPs across the different conditions were plotted as a heat map (red → increase; blue → decrease). **(E)** Nascent RNA imaging of WT, S4A, and S4D myc-Ncl expressing iKras PDAC cells, in presence or absence of $Kras^{G12D}$. Vectors encoding Myc-tagged WT, S4A, and S4D Ncl were transiently transfected into iKras PDAC cells, before reseeding and growing the cells for 48hrs in presence or absence of doxycycline. Cells were then subjected to pulse labeling with FUrd, fixation, and immunostaining with anti-FUrd antibody (green), anti-Myc-tag antibody (red), and Hoechst (blue), followed by confocal microscopy analysis. Scale bar = 10 µm. **(F)** Quantification of FUrd levels in Myc-positive nucleoli from (E). FUrd fluorescence densities in single nucleoli were quantified from 160-281 individual cells per condition, combined from three independent biological replicate experiments (****: P < 0.0001; n.s.: not significant). **(G)** RT-qPCR analysis of 5'ETS-containing pre-rRNA transcript levels in WT, S4A, and S4D myc-Ncl expressing iKras PDAC cells, in presence or absence of $Kras^{G12D}$. Vectors encoding Myc-tagged WT, S4A, and S4D Ncl were transiently transfected into iKras PDAC cells, before reseeding and growing the cells for 48hrs in presence or absence of doxycycline, followed by RT-qPCR analysis with a specific probe against the mouse 5'ETS region. A probe against mouse Actb mRNA was used as loading control for normalization (n = 6) (****: P < 0.0001; n.s.: not significant). **(H)** TMT quantitative analysis of RP levels in WT, S4A, and S4D myc-Ncl expressing iKras PDAC cells, in presence or absence of $Kras^{G12D}$. Vectors encoding Myc-tagged WT, S4A, and S4D Ncl were transiently transfected into iKras PDAC cells, before reseeding and growing the cells for 48hrs in presence or absence of doxycycline. Cells were then lysed and analyzed by TMT-mediated quantitative proteomics. Z-scores of TMT intensity changes for all identified RPs across the different conditions were plotted as a heat map (red → increase; blue → decrease).

Ncl is crucial for Oncogenic Kras mediated PDAC cell proliferation and tumorigenesis

Hyperactive ribosome biogenesis is a hallmark of most malignancies, acting to sustain augmented protein synthesis that underpins unrestricted cancer cell proliferation and tumor growth (Pelletier et al., 2018). We therefore investigated whether the Ncl-mediated enhancement of ribosome biogenesis downstream of $Kras^{G12D}$ was crucial for PDAC proliferation and tumor formation. As demonstrated before (Ying et al., 2012), $Kras^{G12D}$ removal significantly reduced the proliferation of iKras PDAC cells in long-term clonogenic assays under standard 2D cell culture settings (Figure S5A, & S5B). The impact of $Kras^{G12D}$ expression on PDAC cell proliferation was also evident in a 3D matrix made up of collagen-I, which forms the bulk of PDAC extracellular matrix, with rapid proliferative growth of the cell mass into the matrix that was strictly dependent on $Kras^{G12D}$ expression (Figure S5C & S5D). Depletion of Ncl abrogated the effect of $Kras^{G12D}$ in both 2D and 3D culture settings, revealing a strong dependence on Ncl for $Kras^{G12D}$ mediated PDAC cell proliferation (Figure 5A-D).

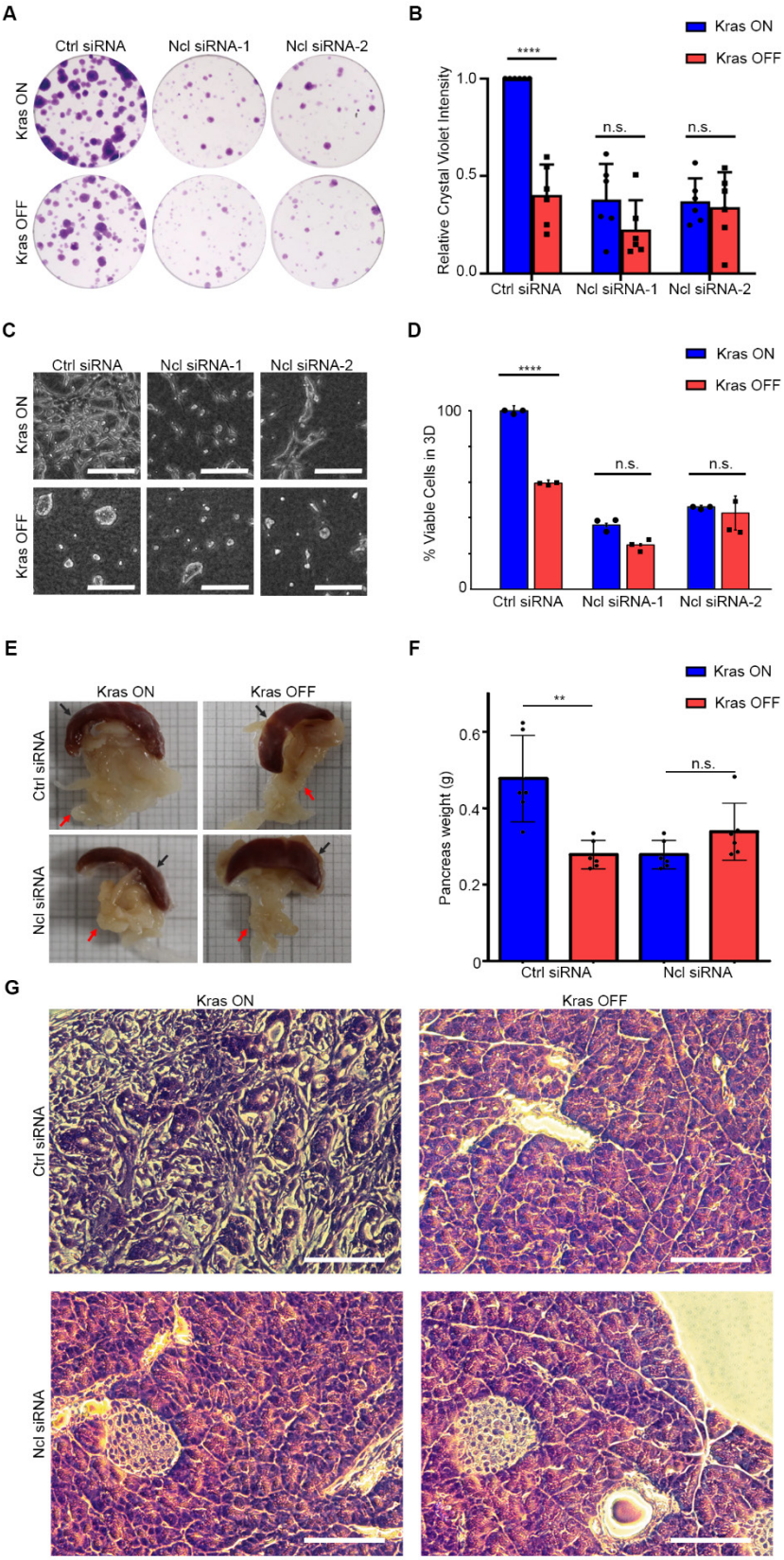

Figure 5: Ncl is necessary for Kras^{G12D}-mediated PDAC cell proliferation and tumor formation. (A) Colony formation of control and Ncl depleted iKras PDAC cells, in presence or absence of Kras^{G12D}. Cells were transfected with a non-targeting control siRNA, or two independent siRNAs against Ncl, followed by clonogenic assay for 7 days in presence or absence of doxycycline. Colonies were visualized by Crystal Violet staining. **(B)** Quantification of Crystal Violet staining levels from (A) (n = 6). (****: P < 0.0001; n.s.: not significant). **(C)** 3D proliferation of control and Ncl depleted iKras PDAC cells, in presence or absence of Kras^{G12D}. Cells were transfected with a non-targeting control siRNA, or two independent siRNAs against Ncl, before being reseeded onto 3D Collagen-I gels, with or without doxycycline, and allowed to grow for 48 hrs. Cells were subsequently imaged live by phase contrast microscopy. Scale bar = 200 µm. **(D)** Analysis of the percentage of viable cells in 3D collagen-I cultures from (C). Cells were subjected to luminescence-based viability assay by CellTiter-Glo to quantify the percentage of viable cells (n = 3) (****: P < 0.0001; n.s.: not significant). **(E)** Representative images of the pancreas from control or Ncl depleted iKras PDAC cells, in presence or absence of Kras^{G12D}. Non-targeting control or Ncl siRNA transfected iKras PDAC cells were orthotopically engrafted into the pancreas of nude mice. Mice were fed either doxycycline-containing (Kras ON) or doxycycline-free (Kras OFF) water for 7 days, before culling and extraction of their pancreas (red arrow). Spleen (black arrow), which is located adjacent to the pancreas, was also extracted and included in the images for comparison. **(F)** Quantification of pancreas weights from (E), as a measure of orthotopic tumor growth. Pancreas weights from a total of 6 animals per condition were quantified. (**: P < 0.01; n.s.: not significant). **(G)** H&E analysis of the extracted pancreas tissues from (E). Extensive portions of the tissue in control engrafted mice fed with doxycycline display PDAC histology, with malignant ductal structures

530 surrounded by stroma. However, typical pancreas histology comprised of acini, islets, and normal ducts is observed in all other conditions. Scale bar = 100 µm.

Using orthotopic xenografts of the iKras PDAC cells, we next investigated whether Kras^{G12D}-induced tumor formation *in vivo* was also dependent on Ncl. Orthotopic xenografts of iKras
535 PDAC cells have been demonstrated to generate tumors which faithfully recapitulate the histological and molecular features of PDAC, in a doxycycline-dependent manner (Ying et al., 2012). In our pilot studies, tumors were fully established within a week of engraftment in doxycycline-fed mice, with animals having to be sacrificed 2-3 weeks post-engraftment due to rapid disease progression (Figure S5E). Thus, we chose a time-scale of one week post-
540 engraftment for investigating the impact of Ncl depletion on Kras^{G12D}-dependent tumor formation. As expected, doxycycline-mediated Kras^{G12D} expression triggered significant tumor growth in the pancreas of the engrafted mice, which was inhibited in the absence of doxycycline. Depletion of Ncl abrogated this Kras^{G12D}-induced tumor formation, demonstrating that Kras^{G12D} function *in vivo* was also reliant on Ncl (Figure 5E, 5F, & S5F).
545 Histological analysis further revealed an extensive Kras^{G12D}-dependent growth of the malignant component and its associated stroma within the pancreas of the engrafted mice, which was completely inhibited upon Ncl depletion (Figure 5G). Collectively, these results reveal that Ncl is crucial for PDAC cell proliferation and tumor formation downstream of Kras^{G12D}.

550

Kras dependency on Ncl-mediated ribosome biogenesis can be therapeutically targeted

Our results reveal a dependency for Ncl in Kras^{G12D}-mediated PDAC tumor formation, suggesting a possibility for therapeutic exploitation. Ncl has been a subject of significant interest as a therapeutic target for a diverse range of cancers, owing to its often strong
555 upregulation of expression combined with its pro-malignancy functions (Abdelmohsen and Gorospe, 2012). However, most efforts so far have been focused on cell-surface localized Ncl, which is commonly observed in cancerous but not normal tissues. Accordingly, several compounds that can target extracellularly localized Ncl have been developed (Abdelmohsen and Gorospe, 2012), but these compounds are unlikely to reach nucleolar Ncl in significant
560 quantities due to lack of cell-permeability. We demonstrated that Ncl is exclusively localized to the nucleolus, associated with pre-rRNA, and functions to promote ribosome biogenesis in iKras PDAC cells. We thereby reasoned that pharmacological inhibition of ribosome biogenesis should functionally mimic Ncl removal in this PDAC model. For this purpose, we utilized CX-5461, the specific RNA polymerase I inhibitor used earlier that can also be orally
565 administered, *in vivo* (Drygin et al., 2011). CX-5461 has shown promising results in early clinical trials against a number of human malignancies (Hilton et al., 2018; Khot et al., 2019). However, its *in vivo* mechanism of action has been subject to some controversy. Early reports suggested that the primary anti-tumor activity of CX-5461 arises from inhibition of ribosome biogenesis (Bywater et al., 2012; Drygin et al., 2011). However, recent studies have revealed
570 that CX-5461 can also induce DNA damage, which seems to act as the primary mechanism of its cytotoxicity (Bruno et al., 2020; Negi and Brown, 2015; Quin et al., 2016; Sanij et al., 2020; Xu et al., 2017). This is thought to be initiated by the irreversible arrest of RNA polymerase I

on rDNA promoter regions, leading to nucleolar stress, which in-turn blocks DNA replication and triggers a genome-wide DNA damage response (Mars et al., 2020). To deconvolute the
575 effects of CX-5461 on rRNA synthesis and DNA-damage, we performed a dose-titration, and assessed the treatment impacts on nascent rRNA expression as well as DNA damage. Short-term treatment of iKras PDAC cells with low nanomolar doses of CX-5461 induced a potent inhibition of nascent rRNA expression (Figure 6A & 6B). This was followed by a significant depletion in the levels of 47S pre-rRNA (Figure 6C). CX-5461 treatment also induced DNA
580 damage in iKras PDAC cells, but this only occurred at the 1 µM dose (Figure S6A & S6B). Consistent with the proposed role of nucleolar stress in this process, 1 µM CX-5461 also caused the disruption of nucleoli, which was not evident at lower nanomolar doses (Figure 6A). Critically, low nanomolar doses of CX-5461 could still abrogate the impact of $Kras^{G12D}$ expression on proliferation of iKras PDAC cells, suggesting that inhibition of rRNA synthesis is
585 the critical target of CX-5461 in the context of $Kras^{G12D}$-driven PDAC cell proliferation (Figure 6D & 6E).

Next, we evaluated the impact of CX-5461 on the proteome of iKras PDAC cells. Similar to $Kras^{G12D}$ removal, nanomolar dose treatment of CX-5461 induced a strong decrease in the
590 levels of Ribosome and rRNA processing protein categories, without affecting protein categories involved in the DNA damage response (Figure S6C & Dataset S12). Accordingly, when combined with $Kras^{G12D}$ induction, this CX-5461 treatment could suppress the $Kras^{G12D}$-induced accumulation of RPs (Figure 6F). Collectively, these results suggest that nanomolar doses of CX-5461 primarily inhibit PDAC cell proliferation via inhibition of $Kras^{G12D}$-driven
595 ribosome biogenesis, with DNA damage occurring only at higher doses. Our findings also highlight that extra care must be taken in choosing the dosage of CX-5461 treatment, in order to achieve a specific inhibition of ribosome biogenesis.

Finally, we assessed whether pharmacological inhibition of ribosome biogenesis by CX-5461
600 could inhibit $Kras^{G12D}$-induced tumor growth, *in vivo*. To mimic therapeutic settings, orthotopic xenograft tumors were first established in doxycycline-fed mice for 4 days, before the animals were subjected to treatment by oral administration of CX-5461 for a further period of 10 days, or left untreated for the same period as control. Magnetic Resonance Imaging (MRI) was used to monitor disease progression for the duration of the experiment.
605 MRI imaging revealed that while tumors grew rapidly in untreated mice, tumor growth was halted in response to CX-5461 treatment (Figure 6G & 6H). End-point analysis of the pancreatic tissues also revealed a significant inhibition of tumor growth in CX-5461 treated mice, with histological analysis showing a strong reduction in the proportion of the malignant component in comparison to untreated animals (Figure 6I-K). Immunohistochemistry (IHC)
610 analysis revealed no evidence of DNA damage in the tumors, suggesting that the *in vivo* CX-5461 dose used in our study (50 mg/kg) is comparable with the *in vitro* low dose treatments which do not induce DNA damage (Figure S6D). Together, these results reveal that pharmacological inhibition of ribosome biogenesis, the critical downstream target of the $Kras^{G12D}$-Ncl axis, could be used as a therapeutic strategy for inhibiting PDAC growth.

615

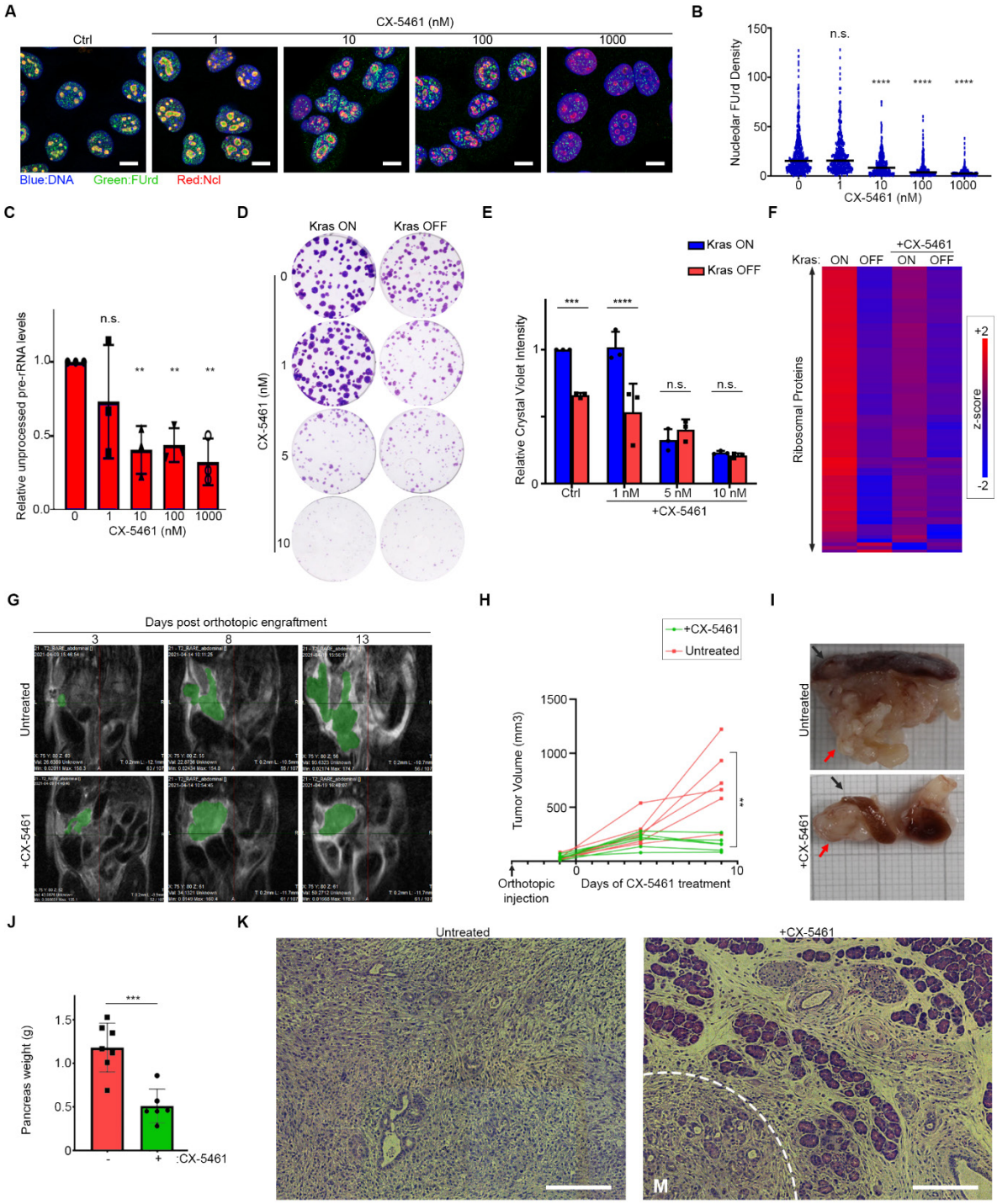

Figure 6: PDAC dependency on Kras^{G12D}-induced ribosome biogenesis can be therapeutically targeted. (A) Dose response analysis of CX-5461 impact on nascent rRNA expression. IKras PDAC cells grown in presence of doxycycline were pre-treated with the indicated concentrations of CX-5461 for 30 mins, before pulse labeling
620 with FUrd. Cells were then fixed and immunostained with anti-FUrd antibody to visualize nascent RNA (green), anti-Ncl antibody to reveal the Nucleolus (red), and Hoechst (blue) as the Nuclear stain, followed by confocal microscopy analysis. Scale bar = 10 µm. **(B)** Quantification of Nucleolar FUrd levels in images from (A). FUrd fluorescence densities in single nucleoli were quantified from 72-147 individual cells per condition, combined from two independent biological replicate experiments (****: P < 0.0001; n.s.: not significant). **(C)** Dose response
625 analysis of CX-5461 impact on 5'ETS-containing pre-rRNA transcript levels. IKras PDAC cells grown in presence of doxycycline were treated overnight with the indicated doses of CX-5461, before RT-qPCR analysis with a specific probe against the mouse 5'ETS region. A probe against mouse Actb mRNA was used as loading control for normalization (n = 3) (**: P < 0.01; n.s.: not significant). **(D)** Dose response analysis of CX-5461 impact on

$Kras^{G12D}$-driven colony formation of iKras PDAC cells. IKras PDAC cells, seeded with or without doxycycline, were subjected to clonogenic assay in presence of the indicated doses of CX-5461 for 7 days. Colonies were visualized by Crystal Violet staining. **(E)** Quantification of Crystal Violet staining levels from (E) (n = 3). (****: P < 0.0001; ***: P < 0.001; n.s.: not significant). **(F)** Quantitative analysis of RP levels in vehicle or 100 nM CX-5461 treated iKras PDAC cells, in presence or absence of $Kras^{G12D}$. IKras PDAC cells were grown for 48hrs, with or without doxycycline, and in presence or absence of 100 nM CX-5461. Cells were then lysed and analyzed by TMT-mediated quantitative proteomics. Z-scores of TMT intensity changes for all identified RPs across the different conditions were plotted as a heat map (red → increase; blue → decrease). **(G)** MRI imaging of orthotopic iKras tumors in untreated or CX-5461 treated mice. IKras PDAC cells were engrafted into the pancreas of doxycycline-fed nude mice and allowed to form tumors for 4 days. Animals were then divided into two groups, with the first group treated by daily oral administration of CX-5461 (50mg/kg) for a further 10 days, whilst the second group was left untreated for the same period. T2 scans were taken on the indicated days, post-engraftment. Green areas mark the tumors. **(H)** Quantification of tumor volumes from (G). For each condition, six animals were engrafted, treated, and monitored by MRI imaging. (**: P < 0.01; n.s.: not significant). **(I)** Representative images of the pancreas (red arrows) from untreated and CX-5461 treated mice in (G), extracted at the end of the treatment (day 14). Spleen (black arrow), which is located adjacent to the pancreas, was also included in the images for comparison. **(J)** Quantification of pancreas weights from (I). Pancreas weight from each animal in the untreated vs. treated group was measured after extraction. (***: P < 0.001; n.s.: not significant). **(K)** H&E analysis of the extracted pancreas tissues from (I). Representative pancreatic tissue images from the untreated and CX-5461 treated mice, showing typical PDAC histology with malignant ductal structures surrounded by stroma in the untreated, but a largely normal pancreas histology with a small PDAC component (region marked M) in the treated mice. Scale bar = 200 µm.

Discussion

As central modulators of post-transcriptional regulation, many RBPs have been shown to play key roles in cancer development and progression (Kang et al., 2020). Direct alteration of RBPs by mutation is relatively rare in cancer (Gebauer et al., 2021), so a key question concerns the mechanistic link between mutations in cancer driver genes and the resulting dysregulation of RBPs. In this study, we used an inducible mouse model of PDAC, combined with a whole-transcriptome quantitative RIC approach, to unbiasedly assess changes in the RBPome in response to induction of oncogenic RAS signaling. Our results reveal a drastic rewiring of the RBPome upon $Kras^{G12D}$ induction, with many conventional RBPs showing an increase in their association with RNA, whilst non-conventional RBPs exhibit decreased association. This switch occurs downstream of ERK1/2, and is achieved not only through modulation of the expression of RBPs, but also their RNA-binding activity. In particular, we reveal a network of nuclear RBPs which include Ncl, whose RNA-binding activity increases upon $Kras^{G12D}$ induction. Several of these RBPs undergo phosphorylation downstream of ERK1/2, and in the case of Ncl, we demonstrate that these phosphorylations act to enhance the RNA-binding activity. On the other hand, little phosphorylation changes were observed on non-conventional RBPs whose RNA-binding activity was reduced upon $Kras^{G12D}$ induction, suggesting that other mechanisms must be at play in regulating their activity. It is tempting to speculate that other types of post-translational modifications may be involved in modulating the activity of these RBPs, but further work will be necessary to define the mechanisms of regulation, as well as the functional significance of these RBPs in the context

of oncogenic RAS signaling. Nevertheless, our study demonstrates that the RNA-binding activity of many conventional and non-conventional RBPs is highly dynamic and subject to regulation by oncogenic signal transduction pathways.

Ribosome biogenesis is a highly coordinated cellular process, which involves step-wise synthesis, processing, modification, and assembly of rRNA and RPs into mature ribosomal subunits (Pelletier et al., 2018). Ncl is known to play a key role in several steps of ribosome biogenesis, from promotion of pre-rRNA synthesis (Cong et al., 2012; Roger et al., 2003), to mediating pre-rRNA processing (Ginisty et al., 1998), and loading of ribosomal proteins onto pre-rRNA (Bouvet et al., 1998). The central RRM domains of Ncl, which mediate its RNA-binding activity, have been shown to be important for enhancing nascent pre-rRNA expression (Storck et al., 2009), suggesting that this enhancement must be at least in part achieved post-transcriptionally. In line with this observation, we reveal that the phospho-dependent enhancement of Ncl RNA-binding activity leads to an increase in nascent pre-rRNA expression. However, while the phospho-mimicking Ncl mutant boosted nascent pre-rRNA levels in the absence of oncogenic RAS, downstream processing of pre-rRNA was blocked, indicating that in order to mediate pre-rRNA processing, Ncl must undergo dephosphorylation. Interestingly, a structural study has led to a model in which Ncl acts as an RNA chaperone, mediating proper folding of pre-rRNA (Allain et al., 2000). Recent data suggests that such nascent RNA folding could be crucial for enhancing RNA polymerase-I elongation rate by inhibiting polymerase backtracking (Turowski et al., 2020). However, to function as an RNA chaperone, the binding of Ncl to pre-rRNA must be dynamic, initially occurring with high affinity to enforce the correct folding, but subsequently switching to a lower affinity to allow the correctly folded pre-rRNA to dissociate. The phospho-regulation of Ncl revealed in this study provides a mechanism for such dynamic regulation. We propose that, by undergoing cycles of phosphorylation and dephosphorylation downstream of RAS signaling, Ncl orchestrates step-wise synthesis, stabilization, and processing of pre-rRNA, ultimately resulting in enhancement of ribosome biogenesis and promotion of tumor cell proliferation (Figure 7).

Hyperactive ribosome biogenesis is a common feature of a wide variety of human cancers, playing a pivotal role in sustaining the growth and proliferation of cancer cells (Pelletier et al., 2018). Pre-rRNA synthesis is considered to be the rate-limiting step in the process of human ribosome biogenesis (Lam et al., 2007). However, mechanisms by which cancer cells upregulate pre-rRNA production are only beginning to be characterized (Arabi et al., 2005; Delloye-Bourgeois et al., 2012; Hannan et al., 2003; Justilien et al., 2017; Prakash et al., 2019; Zhao et al., 2003). Here we reveal that through phospho-regulation of Ncl, oncogenic RAS signaling enhances pre-rRNA expression and ribosome biogenesis. This upregulation is crucial for mediating PDAC cell proliferation and tumorigenesis. Accordingly, depletion of Ncl, or pharmacological inhibition of pre-rRNA expression by CX-5461, results in abrogation of $Kras^{G12D}$-induced ribosome biogenesis, leading to inhibition of PDAC cell proliferation and preventing tumor growth. We confirm that when used at low doses, the anti-PDAC effects of

CX-5461 are mediated by inhibition of ribosome biogenesis, and not DNA damage induction, which can be caused at higher doses. Based on these results, targeting ribosome biogenesis, either alone or in combination with other targeted therapies, appears to be a promising therapeutic avenue against RAS-driven cancers. CX-5461 has shown promise in early clinical trials (Hilton et al., 2018; Khot et al., 2019), and while our results suggest that its use could be therapeutically beneficial against PDAC, more specific inhibitors of rRNA synthesis are likely to be developed in the near future, which may prove to be particularly effective against RAS-driven cancers, but with fewer side effects. In addition, therapeutic inhibition of nucleolar Ncl itself, or its phospho-regulation downstream of RAS, is an alternative attractive strategy worth further exploration.

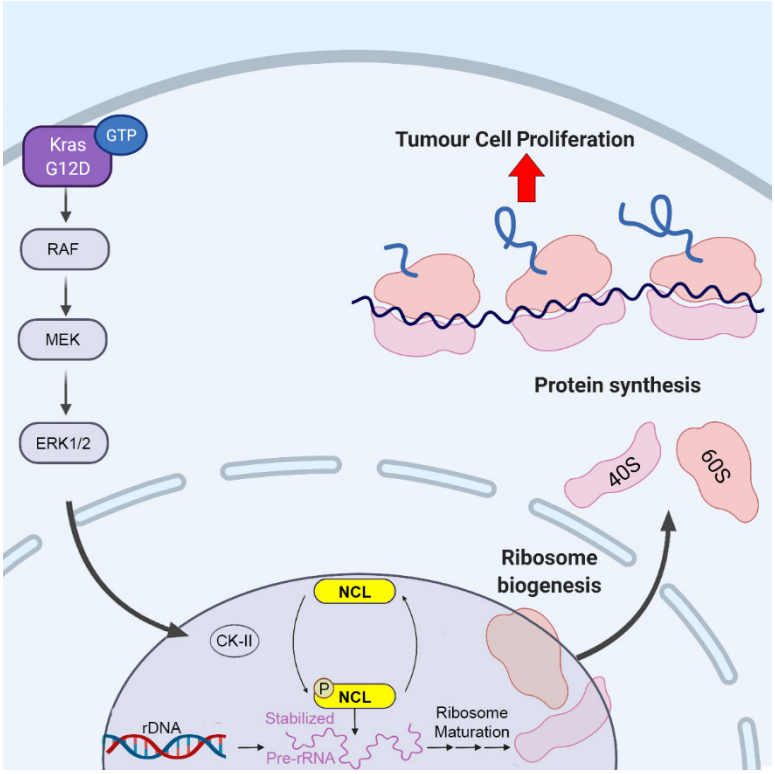

Figure 7: Proposed mechanism of ribosome biogenesis upregulation by oncogenic RAS signaling, via NCL. Oncogenic RAS-induced ERK activity enhances CK2 activity, leading to increased phosphorylation of NCL. This increases the RNA-binding activity of NCL, which acts as a chaperone for nascent pre-rRNA, resulting in its co-transcriptional stabilization and accumulation. NCL then undergoes dephosphorylation, which reduces its RNA-binding activity and enables pre-rRNA to undergo downstream processing and maturation, ultimately leading to enhanced ribosome production that underpins tumor cell proliferation.

Experimental procedures

Data availability information, full list of reagents, and detailed experimental procedures are available in the Supplementary Information.

Author contributions

F.K.M. conceived the study, supervised the work, and wrote the manuscript. M.Dodel. performed the mouse experiments, and the qRIC analyses. F.C. performed the iCLIP experiment. R.F. and J.U. analyzed the iCLIP data. M.Dermit carried out the phospho-proteomics analysis. W.F. assisted with the CK2 activity assessments. M.S.A performed all other experiments and analyzed the data.

Acknowledgements

This work was funded and supported by a Medical Research Council Career Development Award (MR/P009417/1) and a Barts Charity grant (MGU0346) to F.K.M., a Barry Reed PhD studentship to M.S.A., and a Cancer Research UK Centre Grant to Barts Cancer Institute (C355/A25137). We would like to acknowledge the Pre-clinical Imaging facility, the Animal Technician Services (ATS), and the Biological Services Unit (BSU) at Barts Cancer Institute, for their substantial support with the animal work. We would also like to acknowledge the Microscopy, Histopathology, and Mass spectrometry core facilities for their support with imaging and proteomics experiments, and the Barts and the London Genome Centre for the next-generation sequencings. Finally, we would like to thank Dr. Gunnel Hallden for her valuable input on animal experiments, and Dr. Christopher Tape for sharing of reagents and advice on the project.

References

Abdelmohsen, K., and Gorospe, M. (2012). RNA-binding protein nucleolin in disease. RNA Biol *9*, 799-808.

Abdelmohsen, K., Tominaga, K., Lee, E. K., Srikantan, S., Kang, M. J., Kim, M. M., Selimyan, R., Martindale, J. L., Yang, X., Carrier, F.*, et al.* (2011). Enhanced translation by Nucleolin via G-rich elements in coding and non-coding regions of target mRNAs. Nucleic acids research *39*, 8513-8530.

Allain, F. H., Bouvet, P., Dieckmann, T., and Feigon, J. (2000). Molecular basis of sequence-specific recognition of pre-ribosomal RNA by nucleolin. The EMBO journal *19*, 6870-6881.

Angelov, D., Bondarenko, V. A., Almagro, S., Menoni, H., Mongelard, F., Hans, F., Mietton, F., Studitsky, V. M., Hamiche, A., Dimitrov, S., and Bouvet, P. (2006). Nucleolin is a histone chaperone with FACT-like activity and assists remodeling of nucleosomes. The EMBO journal *25*, 1669-1679.

Arabi, A., Wu, S., Ridderstrale, K., Bierhoff, H., Shiue, C., Fatyol, K., Fahlen, S., Hydbring, P., Soderberg, O., Grummt, I.*, et al.* (2005). c-Myc associates with ribosomal DNA and activates RNA polymerase I transcription. Nature cell biology *7*, 303-310.

Baltz, A. G., Munschauer, M., Schwanhausser, B., Vasile, A., Murakawa, Y., Schueler, M., Youngs, N., Penfold-Brown, D., Drew, K., Milek, M.*, et al.* (2012). The mRNA-bound proteome and its global occupancy profile on protein-coding transcripts. Molecular cell *46*, 674-690.

Barbieri, I., Tzelepis, K., Pandolfini, L., Shi, J., Millan-Zambrano, G., Robson, S. C., Aspris, D., Migliori, V., Bannister, A. J., Han, N.*, et al.* (2017). Promoter-bound METTL3 maintains myeloid leukaemia by m(6)A-dependent translation control. Nature *552*, 126-131.

Bouvet, P., Diaz, J. J., Kindbeiter, K., Madjar, J. J., and Amalric, F. (1998). Nucleolin interacts with several ribosomal proteins through its RGG domain. J Biol Chem *273*, 19025-19029.

Bruno, P. M., Lu, M., Dennis, K. A., Inam, H., Moore, C. J., Sheehe, J., Elledge, S. J., Hemann, M. T., and Pritchard, J. R. (2020). The primary mechanism of cytotoxicity of the chemotherapeutic agent CX-5461 is topoisomerase II poisoning. Proceedings of the National Academy of Sciences of the United States of America *117*, 4053-4060.

Bywater, M. J., Poortinga, G., Sanij, E., Hein, N., Peck, A., Cullinane, C., Wall, M., Cluse, L., Drygin, D., Anderes, K.*, et al.* (2012). Inhibition of RNA polymerase I as a therapeutic strategy to promote cancer-specific activation of p53. Cancer Cell *22*, 51-65.

Caizergues-Ferrer, M., Belenguer, P., Lapeyre, B., Amalric, F., Wallace, M. O., and Olson, M. O. (1987). Phosphorylation of nucleolin by a nucleolar type NII protein kinase. Biochemistry *26*, 7876-7883.

810 Castello, A., Fischer, B., Eichelbaum, K., Horos, R., Beckmann, B. M., Strein, C., Davey, N. E., Humphreys, D. T., Preiss, T., Steinmetz, L. M.*, et al.* (2012). Insights into RNA biology from an atlas of mammalian mRNA-binding proteins. Cell *149*, 1393-1406.

Chamousset, D., De Wever, V., Moorhead, G. B., Chen, Y., Boisvert, F. M., Lamond, A. I., and Trinkle-Mulcahy, L. (2010). RRP1B targets PP1 to mammalian cell nucleoli and is associated with Pre-60S
815 ribosomal subunits. Mol Biol Cell *21*, 4212-4226.

Cong, R., Das, S., Ugrinova, I., Kumar, S., Mongelard, F., Wong, J., and Bouvet, P. (2012). Interaction of nucleolin with ribosomal RNA genes and its role in RNA polymerase I transcription. Nucleic acids research *40*, 9441-9454.

de Beus, E., Brockenbrough, J. S., Hong, B., and Aris, J. P. (1994). Yeast NOP2 encodes an essential
820 nucleolar protein with homology to a human proliferation marker. The Journal of cell biology *127*, 1799-1813.

Delloye-Bourgeois, C., Goldschneider, D., Paradisi, A., Therizols, G., Belin, S., Hacot, S., Rosa-Calatrava, M., Scoazec, J. Y., Diaz, J. J., Bernet, A., and Mehlen, P. (2012). Nucleolar localization of a netrin-1 isoform enhances tumor cell proliferation. Sci Signal *5*, ra57.

825 Dermit, M., Dodel, M., Lee, F. C. Y., Azman, M. S., Schwenzer, H., Jones, J. L., Blagden, S. P., Ule, J., and Mardakheh, F. K. (2020). Subcellular mRNA Localization Regulates Ribosome Biogenesis in Migrating Cells. Developmental cell *55*, 298-313 e210.

Drygin, D., Lin, A., Bliesath, J., Ho, C. B., O'Brien, S. E., Proffitt, C., Omori, M., Haddach, M., Schwaebe, M. K., Siddiqui-Jain, A.*, et al.* (2011). Targeting RNA polymerase I with an oral small molecule CX-5461
830 inhibits ribosomal RNA synthesis and solid tumor growth. Cancer research *71*, 1418-1430.

Erard, M. S., Belenguer, P., Caizergues-Ferrer, M., Pantaloni, A., and Amalric, F. (1988). A major nucleolar protein, nucleolin, induces chromatin decondensation by binding to histone H1. Eur J Biochem *175*, 525-530.

Fish, L., Khoroshkin, M., Navickas, A., Garcia, K., Culbertson, B., Hanisch, B., Zhang, S., Nguyen, H. C.
835 B., Soto, L. M., Dermit, M.*, et al.* (2021). A prometastatic splicing program regulated by SNRPA1 interactions with structured RNA elements. Science *372*.

Franceschini, A., Szklarczyk, D., Frankild, S., Kuhn, M., Simonovic, M., Roth, A., Lin, J., Minguez, P., Bork, P., von Mering, C., and Jensen, L. J. (2013). STRING v9.1: protein-protein interaction networks, with increased coverage and integration. Nucleic acids research *41*, D808-815.

840 Garcia-Moreno, M., Noerenberg, M., Ni, S., Jarvelin, A. I., Gonzalez-Almela, E., Lenz, C. E., Bach-Pages, M., Cox, V., Avolio, R., Davis, T.*, et al.* (2019). System-wide Profiling of RNA-Binding Proteins Uncovers Key Regulators of Virus Infection. Molecular cell *74*, 196-211 e111.

Gebauer, F., Schwarzl, T., Valcarcel, J., and Hentze, M. W. (2021). RNA-binding proteins in human genetic disease. Nature reviews Genetics *22*, 185-198.

845 Gerstberger, S., Hafner, M., and Tuschl, T. (2014). A census of human RNA-binding proteins. Nature reviews Genetics *15*, 829-845.

Ginisty, H., Amalric, F., and Bouvet, P. (1998). Nucleolin functions in the first step of ribosomal RNA processing. The EMBO journal *17*, 1476-1486.

Hannan, K. M., Brandenburger, Y., Jenkins, A., Sharkey, K., Cavanaugh, A., Rothblum, L., Moss, T.,
850 Poortinga, G., McArthur, G. A., Pearson, R. B., and Hannan, R. D. (2003). mTOR-dependent regulation of ribosomal gene transcription requires S6K1 and is mediated by phosphorylation of the carboxy-terminal activation domain of the nucleolar transcription factor UBF. Molecular and cellular biology *23*, 8862-8877.

Hentze, M. W., Castello, A., Schwarzl, T., and Preiss, T. (2018). A brave new world of RNA-binding
855 proteins. Nat Rev Mol Cell Biol *19*, 327-341.

Hilton, J., Cescon, D. W., Bedard, P., Ritter, H., Tu, D., Soong, J., Gelmon, K., Aparicio, S., and Seymour, L. (2018). 44O - CCTG IND.231: A phase 1 trial evaluating CX-5461 in patients with advanced solid tumors. Annals of Oncology *29*, iii8.

Hong, S., Freeberg, M. A., Han, T., Kamath, A., Yao, Y., Fukuda, T., Suzuki, T., Kim, J. K., and Inoki, K.
860 (2017). LARP1 functions as a molecular switch for mTORC1-mediated translation of an essential class of mRNAs. Elife *6*.

Ji, H., Wang, J., Nika, H., Hawke, D., Keezer, S., Ge, Q., Fang, B., Fang, X., Fang, D., Litchfield, D. W.*, et al.* (2009). EGF-induced ERK activation promotes CK2-mediated disassociation of alpha-Catenin from beta-Catenin and transactivation of beta-Catenin. Molecular cell *36*, 547-559.
Jumper, J., Evans, R., Pritzel, A., Green, T., Figurnov, M., Ronneberger, O., Tunyasuvunakool, K., Bates, R., Zidek, A., Potapenko, A.*, et al.* (2021). Highly accurate protein structure prediction with AlphaFold. Nature *596*, 583-589.
Justilien, V., Ali, S. A., Jamieson, L., Yin, N., Cox, A. D., Der, C. J., Murray, N. R., and Fields, A. P. (2017). Ect2-Dependent rRNA Synthesis Is Required for KRAS-TRP53-Driven Lung Adenocarcinoma. Cancer Cell *31*, 256-269.
Kang, D., Lee, Y., and Lee, J. S. (2020). RNA-Binding Proteins in Cancer: Functional and Therapeutic Perspectives. Cancers (Basel) *12*.
Khot, A., Brajanovski, N., Cameron, D. P., Hein, N., Maclachlan, K. H., Sanij, E., Lim, J., Soong, J., Link, E., Blombery, P.*, et al.* (2019). First-in-Human RNA Polymerase I Transcription Inhibitor CX-5461 in Patients with Advanced Hematologic Cancers: Results of a Phase I Dose-Escalation Study. Cancer Discov *9*, 1036-1049.
Lam, Y. W., Lamond, A. I., Mann, M., and Andersen, J. S. (2007). Analysis of nucleolar protein dynamics reveals the nuclear degradation of ribosomal proteins. Current biology : CB *17*, 749-760.
Li, D., Dobrowolska, G., and Krebs, E. G. (1996). The physical association of casein kinase 2 with nucleolin. J Biol Chem *271*, 15662-15668.
Linding, R., Jensen, L. J., Pasculescu, A., Olhovsky, M., Colwill, K., Bork, P., Yaffe, M. B., and Pawson, T. (2008). NetworKIN: a resource for exploring cellular phosphorylation networks. Nucleic acids research *36*, D695-699.
Liu, Y., Mattila, J., Ventela, S., Yadav, L., Zhang, W., Lamichane, N., Sundstrom, J., Kauko, O., Grenman, R., Varjosalo, M.*, et al.* (2017). PWP1 Mediates Nutrient-Dependent Growth Control through Nucleolar Regulation of Ribosomal Gene Expression. Developmental cell *43*, 240-252 e245.
Losfeld, M. E., Khoury, D. E., Mariot, P., Carpentier, M., Krust, B., Briand, J. P., Mazurier, J., Hovanessian, A. G., and Legrand, D. (2009). The cell surface expressed nucleolin is a glycoprotein that triggers calcium entry into mammalian cells. Exp Cell Res *315*, 357-369.
Malumbres, M., and Barbacid, M. (2003). RAS oncogenes: the first 30 years. Nat Rev Cancer *3*, 459-465.
Mars, J. C., Tremblay, M. G., Valere, M., Sibai, D. S., Sabourin-Felix, M., Lessard, F., and Moss, T. (2020). The chemotherapeutic agent CX-5461 irreversibly blocks RNA polymerase I initiation and promoter release to cause nucleolar disruption, DNA damage and cell inviability. NAR Cancer *2*, zcaa032.
Matter, N., Herrlich, P., and Konig, H. (2002). Signal-dependent regulation of splicing via phosphorylation of Sam68. Nature *420*, 691-695.
McAlister, G. C., Huttlin, E. L., Haas, W., Ting, L., Jedrychowski, M. P., Rogers, J. C., Kuhn, K., Pike, I., Grothe, R. A., Blethrow, J. D., and Gygi, S. P. (2012). Increasing the multiplexing capacity of TMTs using reporter ion isotopologues with isobaric masses. Analytical chemistry *84*, 7469-7478.
Moudry, P., Chroma, K., Bursac, S., Volarevic, S., and Bartek, J. (2021). RNA-interference screen for p53 regulators unveils a role of WDR75 in ribosome biogenesis. Cell Death Differ.
Negi, S. S., and Brown, P. (2015). rRNA synthesis inhibitor, CX-5461, activates ATM/ATR pathway in acute lymphoblastic leukemia, arrests cells in G2 phase and induces apoptosis. Oncotarget *6*, 18094-18104.
Nusinow, D. P., Szpyt, J., Ghandi, M., Rose, C. M., McDonald, E. R., 3rd, Kalocsay, M., Jane-Valbuena, J., Gelfand, E., Schweppe, D. K., Jedrychowski, M.*, et al.* (2020). Quantitative Proteomics of the Cancer Cell Line Encyclopedia. Cell *180*, 387-402 e316.
Ong, S. E., and Mann, M. (2006). A practical recipe for stable isotope labeling by amino acids in cell culture (SILAC). Nat Protoc *1*, 2650-2660.
Pelletier, J., Thomas, G., and Volarevic, S. (2018). Ribosome biogenesis in cancer: new players and therapeutic avenues. Nat Rev Cancer *18*, 51-63.
Percipalle, P., and Louvet, E. (2012). In vivo run-on assays to monitor nascent precursor RNA transcripts. Methods in molecular biology *809*, 519-533.

Pereira, B., Billaud, M., and Almeida, R. (2017). RNA-Binding Proteins in Cancer: Old Players and New
915 Actors. Trends Cancer *3*, 506-528.
Pichiorri, F., Palmieri, D., De Luca, L., Consiglio, J., You, J., Rocci, A., Talabere, T., Piovan, C., Lagana, A., Cascione, L*., et al.* (2013). In vivo NCL targeting affects breast cancer aggressiveness through miRNA regulation. J Exp Med *210*, 951-968.
Pickering, B. F., Yu, D., and Van Dyke, M. W. (2011). Nucleolin protein interacts with microprocessor
920 complex to affect biogenesis of microRNAs 15a and 16. J Biol Chem *286*, 44095-44103.
Pineiro, D., Stoneley, M., Ramakrishna, M., Alexandrova, J., Dezi, V., Juke-Jones, R., Lilley, K. S., Cain, K., and Willis, A. E. (2018). Identification of the RNA polymerase I-RNA interactome. Nucleic acids research *46*, 11002-11013.
Prakash, V., Carson, B. B., Feenstra, J. M., Dass, R. A., Sekyrova, P., Hoshino, A., Petersen, J., Guo, Y.,
925 Parks, M. M., Kurylo, C. M*., et al.* (2019). Ribosome biogenesis during cell cycle arrest fuels EMT in development and disease. Nat Commun *10*, 2110.
Prior, I. A., Hood, F. E., and Hartley, J. L. (2020). The Frequency of Ras Mutations in Cancer. Cancer research *80*, 2969-2974.
Pylayeva-Gupta, Y., Grabocka, E., and Bar-Sagi, D. (2011). RAS oncogenes: weaving a tumorigenic web.
930 Nat Rev Cancer *11*, 761-774.
Queiroz, R. M. L., Smith, T., Villanueva, E., Marti-Solano, M., Monti, M., Pizzinga, M., Mirea, D. M., Ramakrishna, M., Harvey, R. F., Dezi, V*., et al.* (2019). Comprehensive identification of RNA-protein interactions in any organism using orthogonal organic phase separation (OOPS). Nat Biotechnol *37*, 169-178.
935 Quin, J., Chan, K. T., Devlin, J. R., Cameron, D. P., Diesch, J., Cullinane, C., Ahern, J., Khot, A., Hein, N., George, A. J*., et al.* (2016). Inhibition of RNA polymerase I transcription initiation by CX-5461 activates non-canonical ATM/ATR signaling. Oncotarget *7*, 49800-49818.
Reyes-Reyes, E. M., and Akiyama, S. K. (2008). Cell-surface nucleolin is a signal transducing P-selectin binding protein for human colon carcinoma cells. Exp Cell Res *314*, 2212-2223.
940 Roger, B., Moisand, A., Amalric, F., and Bouvet, P. (2003). Nucleolin provides a link between RNA polymerase I transcription and pre-ribosome assembly. Chromosoma *111*, 399-407.
Sanij, E., Hannan, K. M., Xuan, J., Yan, S., Ahern, J. E., Trigos, A. S., Brajanovski, N., Son, J., Chan, K. T., Kondrashova, O*., et al.* (2020). CX-5461 activates the DNA damage response and demonstrates therapeutic efficacy in high-grade serous ovarian cancer. Nat Commun *11*, 2641.
945 Sengupta, T. K., Bandyopadhyay, S., Fernandes, D. J., and Spicer, E. K. (2004). Identification of nucleolin as an AU-rich element binding protein involved in bcl-2 mRNA stabilization. J Biol Chem *279*, 10855-10863.
Storck, S., Thiry, M., and Bouvet, P. (2009). Conditional knockout of nucleolin in DT40 cells reveals the functional redundancy of its RNA-binding domains. Biol Cell *101*, 153-167.
950 Sysoev, V. O., Fischer, B., Frese, C. K., Gupta, I., Krijgsveld, J., Hentze, M. W., Castello, A., and Ephrussi, A. (2016). Global changes of the RNA-bound proteome during the maternal-to-zygotic transition in Drosophila. Nat Commun *7*, 12128.
Tajrishi, M. M., Tuteja, R., and Tuteja, N. (2011). Nucleolin: The most abundant multifunctional phosphoprotein of nucleolus. Commun Integr Biol *4*, 267-275.
955 Takagi, M., Absalon, M. J., McLure, K. G., and Kastan, M. B. (2005). Regulation of p53 translation and induction after DNA damage by ribosomal protein L26 and nucleolin. Cell *123*, 49-63.
Tape, C. J., Ling, S., Dimitriadi, M., McMahon, K. M., Worboys, J. D., Leong, H. S., Norrie, I. C., Miller, C. J., Poulogiannis, G., Lauffenburger, D. A., and Jorgensen, C. (2016). Oncogenic KRAS Regulates Tumor Cell Signaling via Stromal Reciprocation. Cell *165*, 910-920.
960 Trendel, J., Schwarzl, T., Horos, R., Prakash, A., Bateman, A., Hentze, M. W., and Krijgsveld, J. (2019). The Human RNA-Binding Proteome and Its Dynamics during Translational Arrest. Cell *176*, 391-403 e319.
Tripathi, V., Ellis, J. D., Shen, Z., Song, D. Y., Pan, Q., Watt, A. T., Freier, S. M., Bennett, C. F., Sharma, A., Bubulya, P. A*., et al.* (2010). The nuclear-retained noncoding RNA MALAT1 regulates alternative
965 splicing by modulating SR splicing factor phosphorylation. Molecular cell *39*, 925-938.

Truitt, M. L., Conn, C. S., Shi, Z., Pang, X., Tokuyasu, T., Coady, A. M., Seo, Y., Barna, M., and Ruggero, D. (2015). Differential Requirements for eIF4E Dose in Normal Development and Cancer. Cell *162*, 59-71.

Turowski, T. W., Petfalski, E., Goddard, B. D., French, S. L., Helwak, A., and Tollervey, D. (2020). Nascent Transcript Folding Plays a Major Role in Determining RNA Polymerase Elongation Rates. Molecular cell *79*, 488-503 e411.

Turowski, T. W., and Tollervey, D. (2015). Cotranscriptional events in eukaryotic ribosome synthesis. Wiley interdisciplinary reviews RNA *6*, 129-139.

Ugrinova, I., Petrova, M., Chalabi-Dchar, M., and Bouvet, P. (2018). Multifaceted Nucleolin Protein and Its Molecular Partners in Oncogenesis. Adv Protein Chem Struct Biol *111*, 133-164.

Waters, A. M., and Der, C. J. (2018). KRAS: The Critical Driver and Therapeutic Target for Pancreatic Cancer. Cold Spring Harb Perspect Med *8*.

Wright, C. J., and McCormack, P. L. (2013). Trametinib: first global approval. Drugs *73*, 1245-1254.

Xu, H., Di Antonio, M., McKinney, S., Mathew, V., Ho, B., O'Neil, N. J., Santos, N. D., Silvester, J., Wei, V., Garcia, J.*, et al.* (2017). CX-5461 is a DNA G-quadruplex stabilizer with selective lethality in BRCA1/2 deficient tumours. Nat Commun *8*, 14432.

Ying, H., Kimmelman, A. C., Lyssiotis, C. A., Hua, S., Chu, G. C., Fletcher-Sananikone, E., Locasale, J. W., Son, J., Zhang, H., Coloff, J. L.*, et al.* (2012). Oncogenic Kras maintains pancreatic tumors through regulation of anabolic glucose metabolism. Cell *149*, 656-670.

Yoon, S., and Seger, R. (2006). The extracellular signal-regulated kinase: multiple substrates regulate diverse cellular functions. Growth Factors *24*, 21-44.

Yu, J., Navickas, A., Asgharian, H., Culbertson, B., Fish, L., Garcia, K., Olegario, J. P., Dermit, M., Dodel, M., Hanisch, B.*, et al.* (2020). RBMS1 Suppresses Colon Cancer Metastasis through Targeted Stabilization of Its mRNA Regulon. Cancer Discov *10*, 1410-1423.

Zhang, Y., Bhatia, D., Xia, H., Castranova, V., Shi, X., and Chen, F. (2006). Nucleolin links to arsenic-induced stabilization of GADD45alpha mRNA. Nucleic acids research *34*, 485-495.

Zhao, J., Yuan, X., Frodin, M., and Grummt, I. (2003). ERK-dependent phosphorylation of the transcription initiation factor TIF-IA is required for RNA polymerase I transcription and cell growth. Molecular cell *11*, 405-413.